

High focusing grating reflectors with TE-polarized normal incidence

Ting Ma (马 婷)^{1*}, Xiaodong Yuan (袁晓东)^{1,2}, Weimin Ye (叶卫民)¹, Wei Xu (徐 威)¹,
Shiqiao Qin (秦石乔)^{1,2}, and Zhihong Zhu (朱志宏)^{1,2**}

¹College of Optoelectronic Science and Engineering, National University of Defense Technology,
Changsha 410073, China

²State Key Laboratory of High Performance Computing, National University of Defense Technology,
Changsha 410073, China

*Corresponding author: matingxnew.168@163.com; **corresponding author: zzhwcx@163.com

Received September 17, 2013; accepted December 12, 2013; posted online January 23, 2014

We design two types of reflectors by using subwavelength high-index contrast gratings, which exhibit similar high focusing capabilities at normal incidence with a TE-polarized plane wave. One type has bars of different heights, whereas the other has bars of different depths. Both grating reflectors are designed to be approximately 22 μm in structural length and 10 μm in focal length, at an operating wavelength of 1.55 μm . Both achieve a full-width-half-maximum of 0.9 μm at the focal plane, which is fairly close to the diffraction limit. Their reflectance reach as high as 94% and 91%.

OCIS codes: 050.2770, 050.6624, 050.5080, 230.4040.

doi: 10.3788/COL201412.020501.

Focusing reflectors are among the most fundamental components in applications involving light manipulation, such as imaging, communications, displays, sensing, and lasers. Conventional focusing reflectors are typically curved mirrors made of glass coated with metal, and the focusing power of a reflector arises from its aspheric shape^[1], which presents difficulties in standard microfabrication techniques. However, the integration of focusing element doses require a design that is compatible with standard microfabrication processes, while offering comparable or better performance relative to bulk optics.

Novel types of high-reflectivity, high-index contrast grating (HCG) mirrors have recently been proposed and have become a promising alternative to distributed Bragg reflection dielectric stacks for broadband, high-reflectivity filtering applications^[2–5]. A HCG is a single layer grating comprising high index bars fully surrounded by a low-index medium^[2]. These new types of mirrors are not only more compact and cheaper to fabricate, but also provide unique optical features, such as polarization control^[6]. Non-periodic grating that maintains high-reflectivity can be designed to support a specific phase map for a specific application both numerically and experimentally^[7].

For HCG reflectors with TM-polarized incident light, obtaining a desired phase profile by using purely two-dimensional (2D) scaling with varying the grating period and/or duty cycle (defined as the groove width divided by the grating period) is possible, while maintaining the grating thickness across the entire optic^[7]. Notably, TM-polarized incident light is that in which the E-field vector is perpendicular to the grating bar direction, whereas TE-polarized incident light is that in which the E-field vector is parallel to the grating bar direction.

To our knowledge, no articles have previously discussed HCG focusing reflectors with TE-polarized incident light.

In the process of studying grating focusing reflectors with TE-polarized incident light, we find that to achieve a 2π phase differential within the high-reflectivity region to realize an arbitrary phase distribution, we have no means but to scale the grating thickness. However, this process requires a complex fabrication technique.

In this letter, we introduce two types of HCG focusing reflectors with TE-polarized light at normal incidence. One has bars of different heights, whereas the other has bars of different depths. Both can achieve similar high focusing power.

The HCG reflectors work under a guide-mode resonance (GMR)^[8], which arises when the incident wave couples to a leaky waveguide mode by phase matching with the second-order grating^[9]. The GMR effect is applied to describe the operating principle of the weakly modulated gratings utilizing coupled-wave theory. However, as the index contrast of the grating increases, the solutions arising from the GMR effect applied to describe the HCGs tend to involve heavy mathematical formulation, which is difficult to harness^[10].

A simple analytic analysis of the ultra-high reflectivity feature of HCGs has been previously developed^[11]. The grating bars can be considered as merely a periodic array of waveguides along the z direction (Fig. 1(a)). Upon the plane wave incidence, depending on wavelength and grating dimensions, a few waveguide array modes are excited. The large index contrast and subwavelength dimensions cause a wide wavelength range to exist where only two modes have real propagation constants in the z direction that carry energy. The two modes then depart from the grating input plane ($z = 0$), propagate downward ($+z$ direction) to the grating output plane ($z = t$), and then reflect back up. The higher order modes are typically below cutoff and are in the form of evanescent surface-bound waves. After propagating through the

HCG thickness, each propagating mode accumulates a different phase. At the output plane, a strong mismatch with the output plane wave cause the waveguide modes to not only reflect back to themselves, but also couple into one another. As the modes propagate and return to the input plane, a similar mode coupling occurs. Following the modes through one round trip, the reflectivity solution can be attained. Notably, at the input and output planes, the waveguide modes also transmit out to the air (or more generally to the low-index media). However, the subwavelength period of HCG in open air enables only the zeroth diffraction order to carry energy in reflection and transmission in the form of plane waves. The HCG thickness should be selected such that a destructive interference that cancels transmission is obtained at the output plane.

In the analytical formulation, the TM solution largely relies on the equation $\nabla \times \vec{H} = j\omega\epsilon_0\epsilon_r\vec{E}$, whereas the TE solution greatly relies on the equation $\nabla \times \vec{E} = -j\omega\mu\vec{H}$. The slope of the $\omega - \beta$ curve of TM waveguide modes is significantly different from that of TE waveguide modes near the air light line region; this condition affects the HCG propagation matrix^[12]. All of the above factors largely contribute to the different properties of TE and TM HCGs.

Three physical parameters control the reflective properties of the grating: grating period (p), bar width (w), and grating thickness (t). Figure 1(a) depicts the cross-section view of a uniform grating. The grating bars are made of silicon and surrounded by air located on the substrate of silica. By sweeping the values of parameters p , w , and t , we obtain the whole map of reflectance and phase change of periodic gratings with TE-polarized light at normal incidence. When the grating thickness is fixed at $0.38 \mu\text{m}$ for different grating periods of $p = 0.65, 0.75, 0.85, 0.95,$ and $1.05 \mu\text{m}$, we sweep the bar width w accordingly. We detect the phase of the reflected beam on the surface plane of the grating, which is depicted in Fig. 1(b). Figure 1(c) depicts the reflectance of the gratings.

When the grating thickness is fixed, the phase change diagrams for the different periods are similar to each other (Fig. 1(b)). We also find that when the period is fixed at $1.05 \mu\text{m}$, we can obtain the widest region of high reflectivity (Fig. 1(c)), which also applies to other values of grating thickness. We fix the period of the grating at $1.05 \mu\text{m}$ by scaling the grating thickness and/or duty cycle to achieve a 2π phase differential within a high-reflectivity region. Realizing a full 2π is important because it enables arbitrary phase front control. We conduct our simulations by using a COMSOL Multiphysics RF module based on partial differential equations^[13], and the operating wavelength is $1.55 \mu\text{m}$.

The high index contrast between grating bars and grooves cause the excited modes in HCGs to be strongly confined in the grating bars, where localized resonances occur. The reflective properties at a given point in space thus depend only on the local geometry around that point. The realization that a non-uniform scaling of the reference grating should allow local modulating of the phase value of the reflected beam while maintaining a high reflectivity for a monochromatic incident beam is the critical concept to support the feasibility of designing

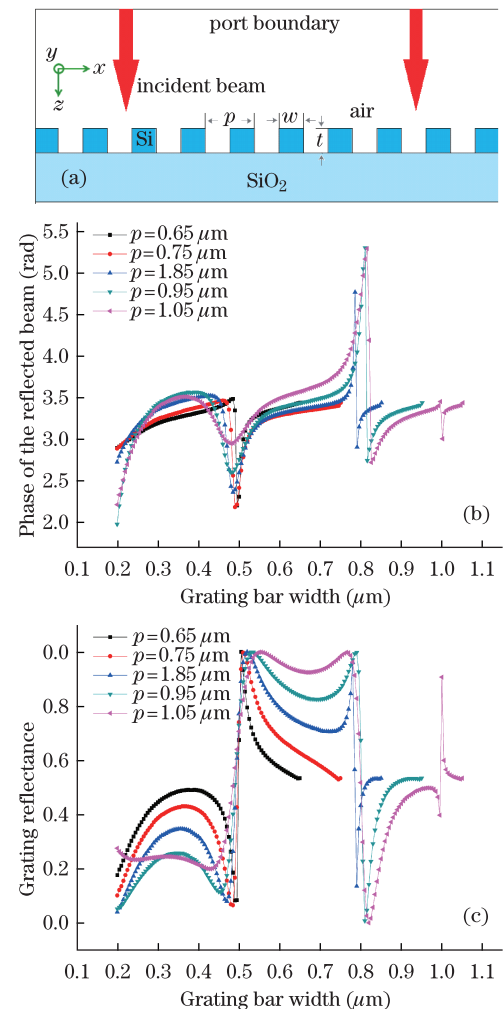


Fig. 1. (a) Schematic drawing of the cross-section of a uniform grating. (b) Phase of the reflected beam and (c) reflectance of a series of periodic gratings. The grating thickness is fixed at $0.38 \mu\text{m}$; for different grating periods of $p = 0.65, 0.75, 0.85, 0.95,$ and $1.05 \mu\text{m}$, we sweep the bar width w accordingly at an operating wavelength of $1.55 \mu\text{m}$.

a non-periodic grating reflector with focusing capabilities. If we want to print a phase $\phi(x)$ on the reflected beam at the position of the grating with transverse coordinates x (for clarity, we focus on 1D grating with period only in the x direction in this letter), we can tune the dimensions of the grating around that position to reach it^[7].

When a wave is incident on a chirped grating reflector, the reflected beam develops a phase distribution along the x axis because of the lateral dimension chirp along the x axis. If the phase distribution is chosen properly, the plane wave is focused. In this letter, we design our needed gratings from a geometrical argument:

$$\phi(x) = \frac{2\pi}{\lambda} \left(f + \frac{\phi_{\max}}{2\pi} \lambda - \sqrt{x^2 + f^2} \right), \quad (1)$$

where f is the focal length, λ is the wavelength, and ϕ_{\max} is the maximum phase change (the phase difference between the middle and the very edge of a focusing element). When the phase $\phi(x)$ is more than 2π , it can be mapped to an equivalent value between 0 and 2π ^[12]. More complicated reflection phase profiles can also be

implemented.

We follow Eq. (1) to calculate and design the grating focusing reflectors that map particular phase profiles on the reflected beam. The next step is to determine a one-to-one correspondence between the complex reflective properties and dimensions of HCGs. Figure 2 shows the phase of the reflected beam and the reflectance of the periodic gratings, of which the period is fixed at $1.05 \mu\text{m}$ and the thickness varies from 0.38 to $0.68 \mu\text{m}$. Figure 2(a) is calculated by setting the port boundary above from the bottom of the grating bar 2λ , that is, it presents the phase change at the bottom of the grating. Figure 2(b) is calculated by the setting port boundary above from the surface of the grating bar 2λ , that is, it presents the phase change on the surface of the grating, and λ is $1.55 \mu\text{m}$. Both Figs. 2(a) and 3(b) show that we cover a full 2π range of phase variation within the high-reflectivity region. We refer to Fig. 2 to search for information related to our design work.

Notably, although the reflection map is calculated for periodic HCGs, its use in arriving at a design for a non-periodic chirped HCG reflector is excellent, as explained in a previous section. In the chirped grating, each bar with a certain bar width and air gap presents a certain phase change corresponding to the relevant uniform grating. Assembling these bars together is equivalent to employing a discrete phase distribution to approximate the ideal continuous phase distribution. The approximation is fairly sufficient because of the subwavelength dimen-

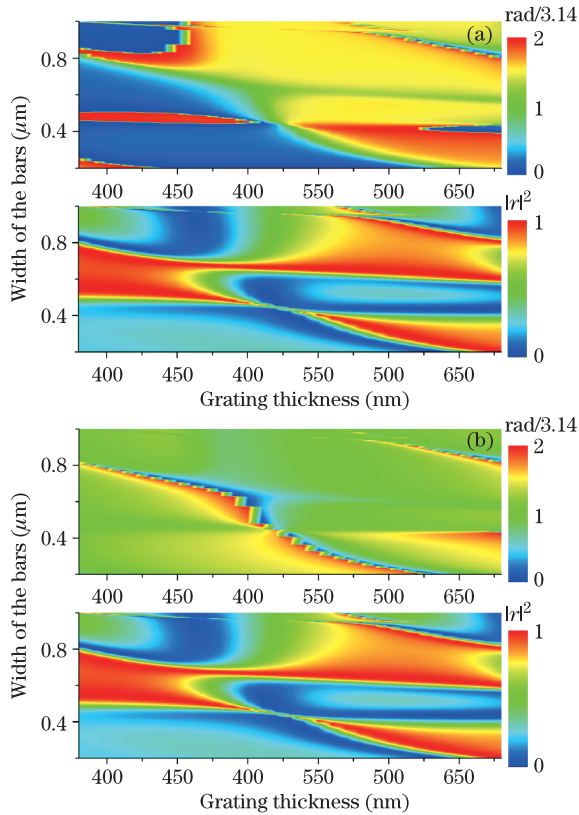


Fig. 2. Phase of the reflected beam and the reflectance of the periodic gratings is plotted as a function of w and t for a fixed grating period of $p = 1.05 \mu\text{m}$ and at an operating wavelength of $\lambda = 1.55 \mu\text{m}$, which is calculated by setting the port boundary above from the (a) bottom and (b) surface of the grating bar 2λ .

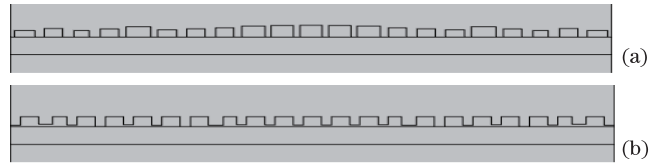


Fig. 3. Schematic of the grating focusing reflector with bars of different (a) heights and (b) depths.

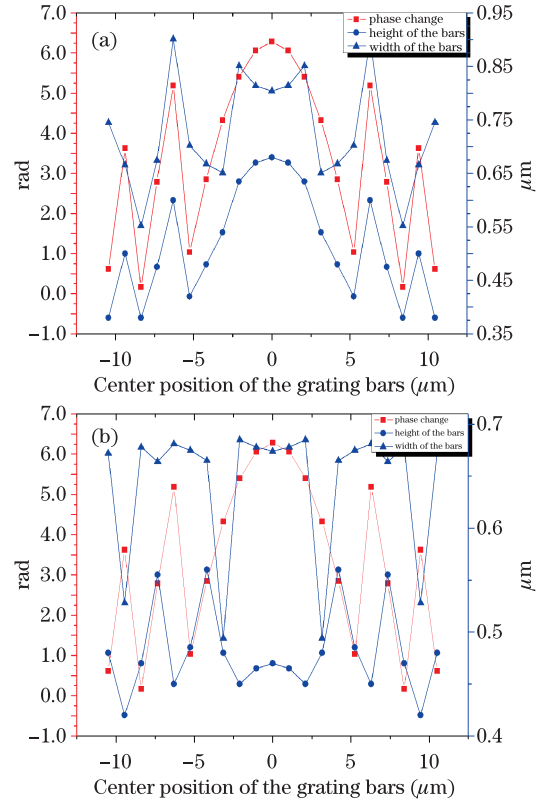


Fig. 4. Detailed structural parameters of (a) A and (b) B and the corresponding phase distributions.

sions of the grating^[14].

Figure 3 depicts the cross-section views of the two grating reflectors we designed; Fig. 3(a) has bars of different heights (A), whereas Fig. 3(b) has bars of different depths (B). Both have similar high focusing capabilities. In designing A , we refer to the data in Fig. 2(a), whereas we refer to the data in Fig. 2(b) in designing B . In Figs. 2(a) and (b), several points relevant to one phase value exist. In the bar-by-bar optimization process, we search for the bar that presents the minimum energy leakage and provides the desired phase change.

Figure 4 shows both the detailed structural parameters and the corresponding phase distributions of A and B . The blue triangles denote the width of the grating bars, the blue dots represent the thickness of the grating bars, and the red squares stand for the phase of the beam reflected by the grating bar. We can see that the phase of the reflected beam exhibits strong correlation with the grating height/depth. This condition exactly confirms the theory described in Refs. [11,12], which we have previously introduced briefly. HCG thickness determines the phase accumulated by the modes and controls their interference, making it one of the most important design parameters.

A notable property of HCGs is that they are scalable with wavelengths. The operating wavelength taken in this work is $1.55 \mu\text{m}$, but the design is scalable to any wavelength. We draw this conclusion based on the property of Maxwell's equations with respect to uniform spatial scale transformation. If we change the spatial dimensions of a periodic grating uniformly by a factor of α , the new reflection coefficient profile is likely similar to that of the original grating, but with a wavelength axis that is also scaled by α . If we design a grating that has a particular reflection coefficient r at a vacuum wavelength λ , we then obtain a new grating with the same reflection coefficient at wavelength λ' by multiplying all grating dimensions by the factor $\alpha = \lambda'/\lambda$ [7].

The focal lengths of both reflectors are designed to be $10 \mu\text{m}$. Figures 5(a) and (b) plots the E-field intensity of the reflected beams of *A* and *B*, respectively. After the plane wave becomes incident from the positive z half-plane, it is reflected mostly by the grating and focused on a spot above the plane, where the reflection occurs from a certain distance of the focal length (Figs. 5(a) and (b)). The total reflectance of *A* is derived as 94% and *B* as 91%. These values are calculated by integrating the power flow of the scattered E-field on the surface above the grating with a short distance dividing the integration of the power flow of the incident E-field.

The two grating focusing reflectors are designed for TE-polarized plane waves at normal incidence, but the concept can be extended to any incident angle in principle^[15].

At the reflection focal plane, the field distribution is shown in Figs. 5(c) and (d); both *A* and *B* represent a full-width-half-maximum (FWHM) of $0.9 \mu\text{m}$, which is fairly close to the diffraction limit. According to the Huygens-Fresnel principle, for a traditional ideal focusing reflector with continuous phase distribution, the FWHM at its focal plane can theoretically be evaluated as $\delta y = 1.22\lambda f/D$ ^[16], where λ is the wavelength, f is the focal length, and D is the aperture of the reflector. As to an ideal focusing reflector with $\lambda = 1.55 \mu\text{m}$, $f = 10 \mu\text{m}$, $D \approx 22 \mu\text{m}$, this reflector corresponds to the HCG reflectors we have designed at $\delta y = 0.86 \mu\text{m}$. The FWHM of *A* and *B* is $0.9 \mu\text{m}$, which is fairly close to $0.86 \mu\text{m}$. The subwavelength structure with discrete phase distribution can achieve high focusing power, which closely approximates the ideal reflector. Note that the field distribution in Fig. 5 is plotted after the incident wave is subtracted from the total field intensity.

As regards the sensitivity of our designs, we perform some further simulation calculations. We find that when the operating wavelength changes by 2%, the focusing power of the grating reflectors significantly decreases; whereas the reflective power remains nearly as high as before. Considering the wavelength scaling property of the HCGs, when the structural parameters change by 2%, similar behavior is observed. The explanation for this phenomenon is straightforward. The high reflectivity of the HCG is broadband, but the operating wavelength or the structural parameters affects the phase accumulation of the reflected beam and then affects the focusing power significantly. The focusing and reflective capabilities of our designs significantly depend on the angle of incidence. When the incidence angle deviates by 1° from

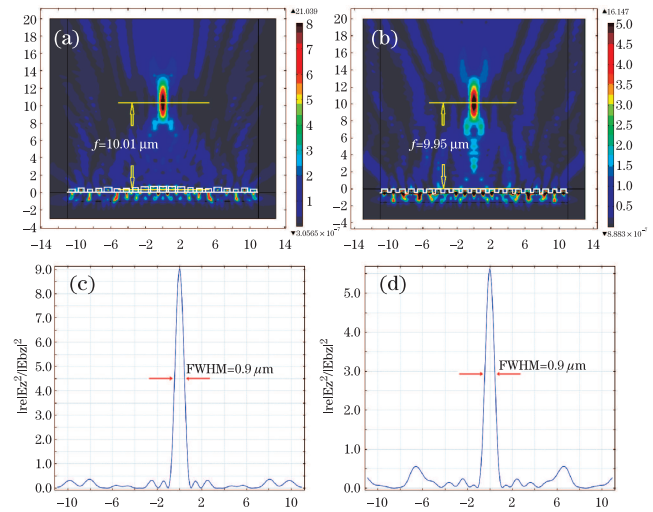


Fig. 5. Visual graph of the E-field intensity for the reflected beam of (a) *A* and (b) *B*. E-field intensity distribution at the reflection focal plane of (c) *A* and (d) *B*.

the normal direction, the focusing capabilities of our designs disappear, and the reflectance significantly decreases.

In the structure of our designs, we have to introduce different grating thicknesses for different grating elements, which impose challenges on the fabrication process^[17]. In this letter, although we have yet to bring our work into the experimental stage we would like to offer two alternative solutions to solve the fabrication problem. We can employ focused ion beam (FIB) applications. FIB milling, implantation, and deposition offer unique and powerful techniques for the fabrication of 3D microstructures. FIB micromachining has high flexibility in the achievable shapes and attainable resolutions (below 100 nm for deposition, even lower for milling and implantation)^[18,19]. We can also approach applications by gray scale photolithography.

In conclusion, in the process of designing subwavelength HCG reflectors with focusing capabilities that are incident with TE-polarized light at a normal direction, we find an intriguing phenomenon. We design two types of grating reflectors: one has bars of different heights, whereas the other has bars of different depths. These two types of grating reflectors own similar high reflectivity and focusing power. As previously mentioned, grating *A* exhibits a reflectance of 94% and FWHM of $0.9 \mu\text{m}$ at the focal plane; grating *B* exhibits a reflectance of 91% and FWHM of $0.9 \mu\text{m}$ at the focal plane. The FWHM of *A* and *B* is fairly close to the diffraction limit.

References

1. E. Hecht, *Optics* (Addison Wesley, 2007) chap. 5.
2. C. F. R. Mateus, M. C. Y. Huang, Y. Deng, A. R. Neureuther, and C. J. Chang-Hasnain, *IEEE Photon. Technol. Lett.* **16**, 518 (2004).
3. C. Mateus, M. Huang, L. Chen, C. Chang-Hasnain, and Y. Suzuki, *IEEE Photon. Technol. Lett.* **16**, 1676 (2004).
4. M. Huang, Y. Zhou, and C. Chang-Hasnain, *Nat. Photon.* **1**, 119 (2007).

5. M. C. Y. Huang, Y. Zhou, and C. J. Chang-Hasnain, *Appl. Phys. Lett.* **92**, 171 (2008).
6. W. Cao, J. Ma, and C. Zhou, *Chin. Opt. Lett.* **10**, 112301 (2012).
7. D. Fattal, J. Li, Z. Peng, M. Fiorentino, and R. G. Beausoleil, *Nat. Photon.* **4**, 466 (2010).
8. J. Wu, C. Zhou, H. Cao, A. Hu, W. Sun, and W. Jia, *Chin. Opt. Lett.* **11**, 060501 (2013).
9. R. Magnusson and M. Shokooch-Saremi, *Opt. Express* **16**, 3456 (2008).
10. S. S. Wang, R. Magnusson, and J. S. Bagby, *J. Opt. Soc. Am. A* **7**, 1470 (1990).
11. V. Karagodsky, F. G. Sedgwick, and C. J. Chang-Hasnain, *Opt. Express* **18**, 16973 (2010).
12. C. J. Chang-Hasnain and W. Yang, *Adv. Opt. Photon.* **4**, 379 (2012).
13. Z. H. Zhu, W. M. Ye, J. R. Ji, X. D. Yuan, and C. Zen, *Appl. Phys. B* **86**, 327 (2007).
14. F. Lu, F. G. Sedgwick, V. Karagodsky, C. Chase, and C. J. Chang-Hasnain, *Opt Express* **18**, 12606 (2010).
15. Y. Zhou, M. C. Y. Huang, C. Chase, V. Karagodsky, M. Moewe, B. Pesala, F. G. Sedgwick, and C. J. Chang-Hasnain, *IEEE J. Sel. Top. Quantum Electron.* **15**, 1485 (2009).
16. G. Brooker, *Modern Classical Optics* (Oxford University, 2003).
17. L. Ge, X. Wang, H. Chen, K. Qiu, and S. Fu, *Chin. Opt. Lett.* **10**, 090502 (2012).
18. S. Reyntjens and R. Puers, *J. Micromech. Microeng.* **11**, 287 (2001).
19. Z. H. Zhu, C. C. Guo, K. Liu, W. M. Ye, X. D. Yuan, B. Yang, and T. Ma, *Opt. Lett.* **37**, 698 (2012).